Lunar Relay Onboard Navigation Performance and Effects on Lander Descent to Surface

Jeffrey L. Small, Laurie M. Mann, Juan M. Crenshaw, Cheryl J. Gramling, Jose J. Rosales, Luke B. Winternitz, Munther A. Hassouneh, Dahlia A. Baker, Sun Hur-Diaz, Andrew J. Liounis, *NASA Goddard Space Flight Center*

BIOGRAPHIES

Jeffrey Small is a flight dynamics engineer working in NASA Goddard Space Flight Center's Navigation and Mission Design Branch since 2020. His work focuses on orbit determination in the Lunar regime.

Laurie Mann is a flight dynamics engineer working for NASA Space Flight since 2000. She recently joined the Navigation and Mission Design Branch working on mission design, navigation, and technology development activities in support of the Artemis program.

Juan Crenshaw is a member of the Navigation and Mission Design Branch at NASA Goddard Space Flight Center. He is involved in technology development efforts in support of lunar navigation.

Cheryl Gramling is the Associate Chief for Technology in the Mission Engineering and Systems Analysis Division at GSFC, and is the position, navigation, and timing subject matter expert on the Lunar relay system.

Jose J. Rosales is a Flight Dynamics Engineer at the NASA Goddard Space Flight Center. Since 2013 he supported the James Webb Space Telescope as a Systems Engineer. He is currently working on Lunar and libration point missions as a trajectory designer.

Luke Winternitz is a navigation engineer working in NASA Goddard Space Flight Center's Components and Hardware Systems Branch since 2001. His work focuses on space GNSS receiver and navigation software development, testing, and analysis.

Dr. Munther Hassouneh is a senior engineer at Goddard Space Flight Center. He joined NASA in 2010 and has focused on GNSS receiver technology development and miniaturization. He is currently the lead for the lunar GNSS receiver.

Dahlia Baker is a PhD student at the University of Colorado Boulder and a pathways intern at NASA Goddard Space Flight Center. Her work focuses on shape modeling and optical navigation for small body exploration.

Sun Hur-Diaz is a member of the Navigation and Mission Design Branch at NASA Goddard Space Flight Center. She specializes in space trajectory optimization and autonomous navigation technologies.

Andrew Liounis is an Aerospace engineer in the Navigation and Mission Design Branch at NASA's Goddard Space Flight Center. He is the primary author of the open-source Goddard Image Analysis and Navigation Tool (GIANT) and specializes in optical navigation, orbit determination, and software development.

ABSTRACT

A system of Lunar relay satellites has been proposed to address communication and navigation needs and ensure robustness for the variety of upcoming robotic and human exploration missions to the Moon. The relays are envisioned to estimate self-position and time knowledge onboard, allowing the system to provide in-situ navigation services to missions in the Lunar and cis-Lunar environment. The quality and accuracy of those services are highly dependent on the navigation performance of the relay itself. To assess the Lunar relay navigation performance, a series of orbit determination (OD) Monte Carlo (MC) simulations are run using Lunar gravity modeling up to a degree and order of 250 and a variety of onboard clocks and measurement types including weak-signal GNSS, Ground Network (GN) pseudorange (PR) and Doppler, and optical navigation (OpNav) center-finding (CF). The estimated trajectories produced by these Lunar relay MC simulations, along with

the associated errors, and transmitted navigation reference signal parameters, are used to evaluate the expected navigation performance of a user on a descent trajectory to the Lunar surface. The scenario features a lander system performing onboard navigation relying on one-way range and Doppler measurements from reference signals emitted by the Lunar relay. This paper can be used as a reference in determining the onboard clock and measurement types necessary to obtain acceptable navigation performance for the Lunar relay, and as a baseline for Lunar lander navigation performance using accurate measurements from a relay reference signal.

INTRODUCTION

Given the upcoming Artemis program that plans to bring a multitude of robotic missions and land humans back on the Moon, and the expected increased Lunar activities that follow, the need for a navigation-supporting infrastructure at the Moon has become evident to meet mission requirements. LunaNet is an interoperability specification being developed addressing the emerging architectures consisting of a group of relay spacecraft that provide communication and navigation services [1]. One of the notable navigation services included is the ability to provide a reference signal on a proximity link that is structured to enable recipients to measure one-way pseudorange (PR) and Doppler, similar to GNSS measurements in the Earth regime. Spacecraft providing navigation services in orbit around the moon are referred to within this study as Lunar Navigation Nodes (LNN). In contrast to Earth based measurement observables, LNN observables provide navigation knowledge in the Lunar frame, which could be invaluable in helping to meet mission requirements, particularly for Lunar landers [2].

There are a variety of Lunar orbits being considered for the LNN, and no one orbit scheme is mandated. To reduce scope, the LNN orbit analyzed and presented in this work is a frozen orbit with a twelve-hour orbital period. The orbit is designed to maintain coverage of the Lunar south pole, with coverage varying from 60-80% of the time for users between the latitudes of 45 and 90 degrees south. Additionally, the frozen nature of the orbit means it requires only yearly maneuvers to maintain.

This study is divided into two distinct analyses, with the first focusing on LNN self-navigation state and time knowledge. To provide useful measurements, the LNN must have an accurate estimate of its own state to mitigate ephemeris knowledge errors. The LNN satellites should be designed to run onboard navigation software that processes one-way measurement observables to obtain the most up-to-date and accurate state knowledge. These observables can include GN, OpNav CF, GNSS and crosslink (Xlink) measurements between two different relays. This study focuses on analyzing performance and usefulness in an early deployment scenario, where potentially only one LNN is available, hence crosslink measurements between LNN have not been included. With an LNN relying on one-way measurements, the onboard clock accuracy has a large impact on performance. Any errors in estimating clock biases and clock bias rates will have an impact on the state estimation and cause biases in the reference signals provided to users. The ability to maintain accurate time knowledge onboard is highly dependent on the choice of onboard clock, the measurement observables being processed, and the fidelity of the clock model.

The second analysis conducted as part of this study investigates the navigation performance of a Lunar lander that utilizes the navigation reference signal provided by a single LNN satellite. The analysis was run using a lander descent trajectory to the Lunar surface performing onboard OD using Terrain Relative Navigation (TRN), GN and LNN provided PR and Doppler observables.

To perform the analyses of the LNN self OD and Lunar lander navigation performance, the Goddard Enhanced Onboard Navigation System (GEONS) flight software was utilized through the GEONS Ground MATLAB Simulation (GGMS) interface, which provides GEONS with the appropriate measurement simulations for each scenario [3]. Monte Carlo simulations were run for both the LNN self OD and lander scenarios.

In this paper we describe the simulation setup and present results, showing the impact of the selection of onboard clock hardware and types of measurement observables contributing to the navigation and timing performance of the LNN. Likewise, the simulation setup and results are presented assessing the impact on the navigation errors for an LNN relay user on a descent trajectory to the Lunar surface.

GEONS GROUND MATLAB SIMULATION

GEONS is an onboard navigation software that has been flown on several missions including the Magnetospheric Multiscale Mission (MMS) and the Station Explorer for X-ray Timing and Navigation Technology (SEXTANT) [4]. It utilizes an Extended Kalman Filter (EKF) to process measurements to obtain a spacecraft state estimate at each measurement update.

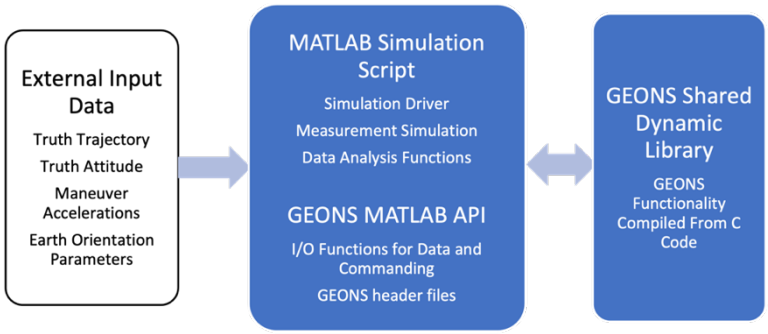
The GEONS Ground MATLAB Simulator (GGMS) was developed to run navigation analyses using GEONS through a MATLAB API. The structure of the GGMS is shown in *Figure 1*. It consists of a collection of MATLAB scripts that control data simulation and processing, the GEONS flight software compiled into a dynamic library, and the MATLAB API that is used to directly call the GEONS flight software. The GEONS flight software is used to propagate the trajectory and covariance, simulate and process measurements, and perform state and covariance updates. GGMS utilizes a truth spacecraft, which is taken from the truth trajectory or propagated from an initial state, and an estimated spacecraft whose state is updated at each measurement update using the EKF. The simulation procedure at each time step is as follows.

1. Propagate the truth and estimated spacecraft trajectory to current timestep
2. Simulate measurements based on the truth spacecraft state
3. Add noise and biases to measurements
4. Process measurements with the EKF, update estimated state estimate

The errors reported by the GGMS are given by the difference between the estimated and truth spacecraft trajectories.

The GGMS has the capability to simulate a wide range of measurements observables. This analysis utilizes weak-signal GPS, OpNav center-finding (CF), TRN, GN, and LNN signal observables. The assumptions for each observable are described in the following sections.

Figure 1: GGMS structure



WEAK-SIGNAL GPS TRACKING

Though originally designed for terrestrial and Lower Earth Orbit (LEO) application, GPS-based space navigation has been extended to apply to users at much higher altitudes. Missions including MMS have demonstrated the effectiveness of weak-signal GPS tracking at distances as far as 29.34 RE or 50% of Lunar distance [5]. Though the LuGRE mission will soon use GPS data at the Moon, there is currently no mission data using GPS at Lunar distances to inform the GGMS models [6]. To account for this, the GGMS incorporates MMS flight data to model how the GPS signal is degraded based on distance to extend GPS modeling to Lunar distances. In addition, data from the Antenna Calibration Experiment (ACE) is used to model the transmit patterns for the GPS antenna based on the azimuth and elevation of the GPS transmitter [7]. The noise of GPS measurements in the simulation is dependent on the GPS-to-receiver link signal to noise ratio (C/N_0) given by *Equation 1*.

$$\frac{C}{N_0} = P_T + G_T(\phi,\theta) - 20\log\left(\frac{4\pi}{\lambda_{L1}}\right) + G_R(\phi,\theta) - L_{pol} - 10\log\left(kT_{sys}\right) - R_{loss} \quad (1)$$

Where λ_{L1} is the GPS L1 carrier wavelength, k is the Boltzmann constant, G_T is the transmitter antenna gain pattern taken from the ACE datasets, and G_R is the receiving antenna gain pattern that models a high gain antenna with a peak gain of 14dBi in the ecliptic plane. The remaining parameters are given in *Table 1*.

Table 1: Calibrated link parameters from analysis of MMS-Navigator GPS receiver and high-altitude flight data

Link Parameter	Value
Antenna Noise Temperature T_a	34 K
System Noise Temperature T_{sys}	132 K
Implementation Loss R_{loss}	1.7 dB
Polarization Loss L_{pol}	1 dB
Block II/IIA P_T (max EIRP)	17.9 dBW (31.6 dBW)
Block IIR P_T (max EIRP)	17.3 dBW (29.2 dBW)
Block IIRM P_T (max EIRP)	18.8 dBW (32.1 dBW)
Block IIF P_T (max EIRP)	16.2 dBW (29.5 dBW)

Only GPS signals with a C/N_0 above 23 dB-Hz were used in the simulation, a maximum of 12 GPS measurements were available at each timestep and only GPS PR measurements were used. Multipath errors were not included in this analysis.

The noise for the GPS PR measurement in the simulation is a function of C/N_0 given by the formula shown in *Equation 2* for thermal noise represented in meters where c is the speed of light, T_c is the code chip duration, B_{dll} is the delay lock loop (DLL) bandwidth, d is the early/late correlator spacing in chips, and T is the coherent integration time [8]. The values used for each parameter are shown in *Table 2*.

$$\sigma = cT_c \sqrt{\frac{B_{dll}d}{2\frac{C}{N_0}}\left(1 + \frac{2}{(2-d)T\frac{C}{N_0}}\right)} \tag{2}$$

Table 2: GPS thermal noise parameters

Link Parameter	Value
T_c	9.7752e-07 s
B_{dll}	1.0 Hz
d	1.0 chip
T	20.0 ms

OPNAV CF AND TRN OBSERVABLES

OpNav observables are extracted by matching a reference template of the target body or feature being imaged with images of the actual body or feature. While the GGMS does not have the capability to simulate images and extract OpNav observables, it can provide analogous navigation data using the relative position between the spacecraft camera and the target to compute both bearing and range measurements. GGMS can simulate both OpNav CF measurements, that is measurements relative to the center of figure of a body, and TRN measurements which are relative to a series of landmarks on the surface of the body being imaged. The noise on the range and bearing measurements is dependent on the camera being used. For this simulation, the camera was assumed to be similar to NavCam 1 used on the OSIRIS-REx mission, with a maximum field of view (MFOV) of 40 deg and a pixel scale of 0.02 deg [9].

Table 3 shows the parameters used for generating CF and TRN observables which are based on navigation experience from the OSIRIS-REx mission and expected performance given currently available systems. A measurement update period of 60 seconds was chosen to account for the computational time needed to process each image onboard. For TRN measurements, landmarks were generated along the descent trajectory so that approximately 3-6 landmarks were visible at each measurement

update. Illumination constraints were not considered. A bias was added to the TRN measurements to account for potential attitude errors during descent.

Table 3: OpNav measurement simulation parameters

OpNav Parameter	Value
CF Operating Range	> 300 km
CF Bearing 1-σ Noise	1 pixel
CF Bearing 1-σ Bias	0 pixels
CF Range 1-σ Noise	0.02% of range to Lunar surface
TRN Max Number of Landmarks	6
TRN Operating Range	0 - 300 km
TRN Bearing 1-σ Noise	3 pixels
TRN Bearing 1-σ Bias	0.5 pixels
Measurement Update Period	60 seconds

GN OBSERVABLES

Simulated one-way GN PR and Doppler data from the Canberra, Madrid, and Goldstone DSN tracking sites were included using the parameters shown in *Table 4.*

Table 4: **GN measurement simulation parameters**

GN Parameter	Value
DSN Frequency	X-band
PR 1-σ Noise	0.32 m
PR 1-σ Bias	15 m
Doppler 1-σ Noise	$0.1 \frac{\text{mm}}{\text{s}}$
Doppler 1-σ Bias	$0 \frac{\text{mm}}{\text{s}}$
Measurement Update Period	10 seconds
LNN Meas Schedule	One 4-hour Pass Per Day
Lander Meas Schedule	Constant Coverage

The PR and Doppler noise values are standard DSN 1-σ values for X-band for a 10-second integration period. The large PR bias was included to be conservative as large biases are possible with one-way GN measurements due to different time and frequency reference sources at the transmit and receive nodes of the measurement.

LNN REFERENCE SIGNAL OBSERVABLES

To provide services to LNN relay users, each LNN transmits reference signals. Analogous to GNSS, these specifically structured signals enable recipients to measure PR and Doppler and time transfer, which can then be processed for position, velocity, and time determination (PVT). Since the signal originates on an orbiting platform, the measurements are modeled as crosslink (orbiting transmitter to orbiting or landed receiver) observables in GEONS. By doing so, ephemeris errors on the LNN are considered in the PVT solution for the receiver.

Simulated one-way LNN reference signal measurements were included only in the lander descent analysis using the measurement parameters shown in *Table 5*. The clock bias errors from the LNN self-OD were added to a baseline value of 0.65 meters for the LNN reference signal PR measurements. No bias is added to the LNN reference signal Doppler measurements, which is consistent with the frequency stability of the reference signal from the LNN.

Table 5: **LNN measurement simulation parameters**

LNN Parameter	Value
Broadcast Frequency	S-band
PR 1-σ Noise	0.32 m
PR 1-σ Bias	RSS of 0.65 m nominal plus LNN clock bias
Doppler 1-σ Noise	$0.16\ \frac{\text{mm}}{\text{s}}$
Doppler 1-σ Bias	$0\ \frac{\text{mm}}{\text{s}}$
Measurement Update Period	10 seconds
Lander Meas Schedule	Constant when in view

Figure 2 and *Figure 3* show the baseline measurement schedule for the LNN relay self-OD and lander descent cases respectively. The plots include measurements from the 12 GPS channels (GPS channel #), the three Earth ground stations (GN-mad, -can, -gold), TRN (TRN), and the LNN reference signal link to the lander (XLINK-LNN).

Figure 2: LNN relay measurement schedule

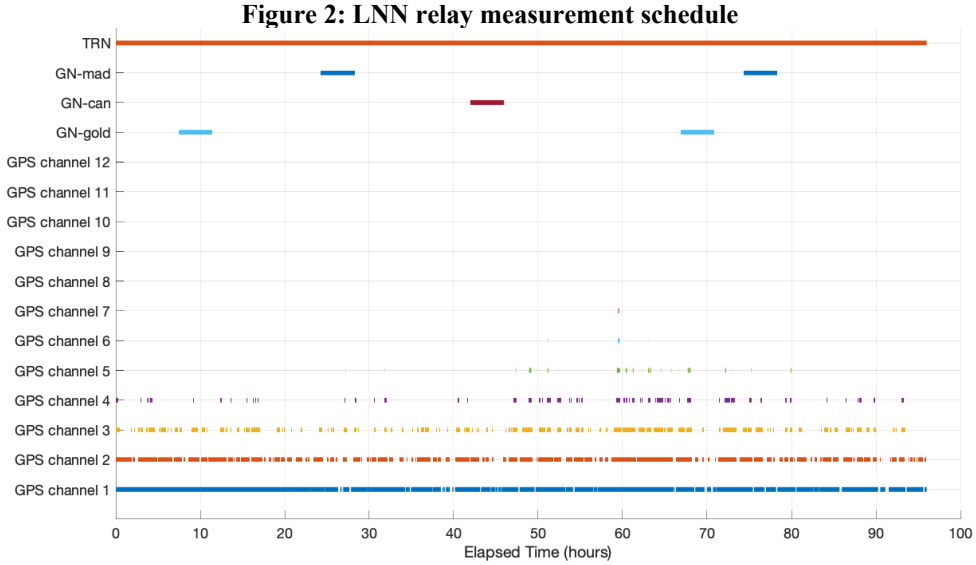
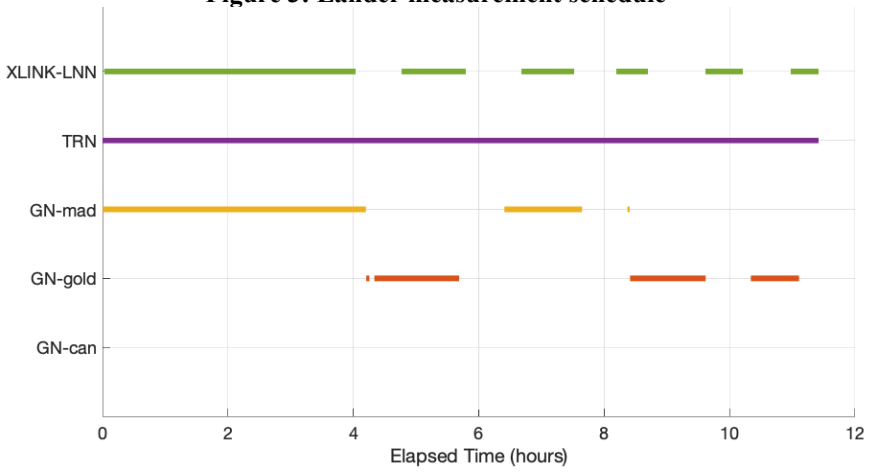


Figure 3: Lander measurement schedule



DESCENT TRAJECTORY

The descent trajectory was generated to meet constraints developed by NASA for a potential Human Landing System (HLS) trajectory. The mission chronology is as follows.

1. Depart a near-rectilinear halo orbit (NRHO) with a maneuver at Apoapsis and target a 100x100 km low Lunar orbit (LLO)
2. Attain LLO (Lunar Orbit Insertion (LOI)) and perform three revolutions
3. Reduce LLO altitude from 100 km to 15 km
4. Perform departure burn from 15 km altitude
5. Perform a series of maneuvers targeting a landing at the Lunar south pole

All maneuvers are modeled as impulsive for ease of implementation. The choice of impulsive or finite maneuver modeling is not expected to have a large effect on the navigation results. An accelerometer is assumed to be onboard the lander that limits the 1-σ DV error to 0.15**%** of the total magnitude for each maneuver.

ON-BOARD CLOCK MODELS

For each scenario studied, two different spacecraft clocks are modeled in this analysis, a Rubidium Atomic Frequency Standard (RAFS) and an Ultra-Stable Oscillator (USO). To model the errors from each clock an integrated white noise process is used with intensities given by q_1, q_2, q_3 for the clock bias, rate, and acceleration, respectively. This same noise model is used for GPS clocks as shown in [10] where the authors give the Hadamard variance ${\sigma_H}^2(\tau)$ produced by the model at interval τ

$$ {\sigma_H}^2(\tau) = q_1\tau^{-1} + \frac{1}{6}q_2\tau + \frac{11}{120}q_3\tau^3 \tag{4} $$

Using *equation 4,* the q-parameter model is fit to RAFS and USO stability data. *Table 6* gives the resulting q parameters.

Table 6: Clock stability (q) parameters

Clock	q_1	q_2	q_3
RAFS	3.70e-24	1.87e-33	7.56e-59
USO	2.53e-23	4.22e-24	1.00e-38

LNN RELAY OD

To assess the navigation performance for a relay in the 12-hour frozen orbit, a series of MC simulations were conducted using various combinations of measurement observables and spacecraft clocks. *Table 7* gives the force modeling assumptions used for the truth and estimated trajectory simulations. The gravity model used for both the truth and estimated trajectories is the GRGM900C model from the Gravity Recovery and Interior Laboratory (GRAIL) mission [11]. The overall scale factor for the force from Solar Radiation Pressure is represented by Cr.

Table 7: Force modeling

Parameter	Truth Trajectory	Estimated Trajectory
Planetary Ephemeris	JPL DE421 [12]	JPL DE421
Solar System Gravity	Point Mass Sun, Earth, Venus, Mars, Jupiter, Saturn	Point Mass Sun, Earth, Venus, Mars, Jupiter, Saturn
Lunar Gravity Model	250x250 GRGM900C	100x100 GRGM900C
Solar Radiation Pressure	Mass = 273.85 kg Area = 4.76709 m^2 Cr = 1.2	Mass = 273.85 kg Area = 4.76709 m^2 Cr = 1.2

To account for potential mismodeling or truncation of the Lunar gravity field by an onboard processor, a higher order field is used for truth than for the estimated trajectory. *Table 8* shows the parameters being varied with each MC sample along with their errors. The errors were sampled following a Gaussian distribution. The parameters estimated for the LNN relay MC analysis include the initial state, GN PR biases, spacecraft Cr, clock bias, clock rate, and clock acceleration.

Table 8: Parameters varied in each LNN relay MC sample

Parameter	Error Applied (1-σ)
Initial Position	10 km
Initial Velocity	10 $\frac{\text{cm}}{\text{s}}$
Initial Clock Bias	3,000 km (1 ms)
Initial Clock Bias Rate	3 $\frac{\text{m}}{\text{s}}$
Initial Clock Bias Acceleration	3e-07 $\frac{\text{m}}{\text{s}^2}$
Spacecraft Mass	0.91 kg
Spacecraft Area	0.16 m^2
Spacecraft Cr	0.1
GN PR Bias (per-pass)	15 m

To ensure filter stability, state process noise and filter measurement multipliers are used. The measurement multipliers increase the predicted noise of the measurement in the filter so noisy measurements are less likely to destabilize the EKF.

For each case, 100 MC iterations were run. 100 MC iterations were chosen to capture a relevant sample of the worst-case errors while still limiting the amount of processing time required to run each case. GPS outages near Perilune were included in some cases to determine the extent to which it degrades the state and clock estimates and to assess the benefits of OpNav CF measurements during outages.

Figure 4 shows the MC RSS position and velocity errors for a MC run using a RAFS clock with GPS, OpNav CF and GN observables and *Figure 5* shows the clock bias and clock rate MC errors for the same case. Each grey line represents a single MC run and the green line represents the 3-sigma envelope across the 100 samples. The MC errors are well aligned with the 3-σ filter covariance and there are no significant outliers.

Figure 4: MC RSS position (top) and velocity (bottom) errors for LNN: RAFS clock, GPS, OpNav CF, and GN measurements

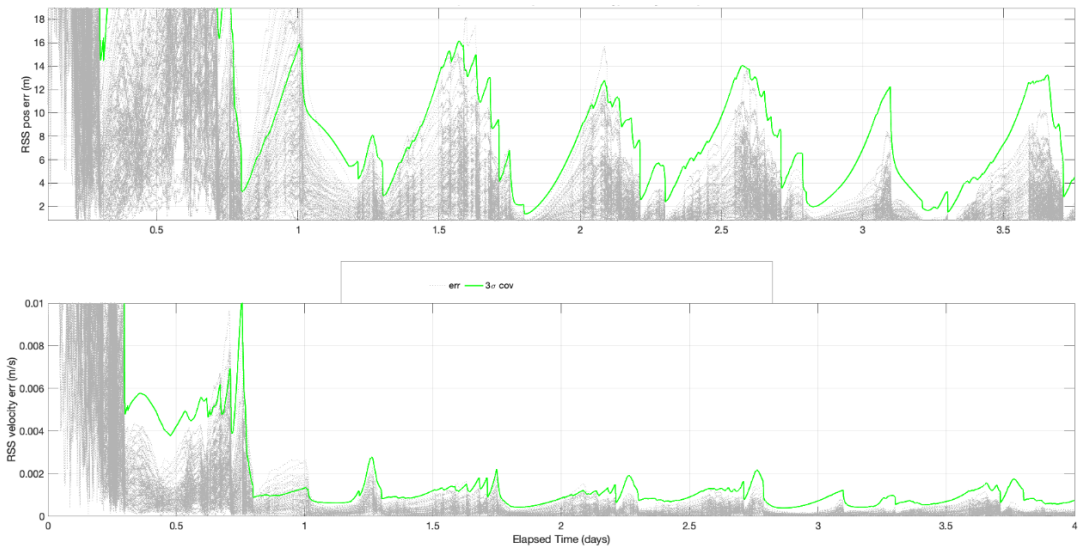
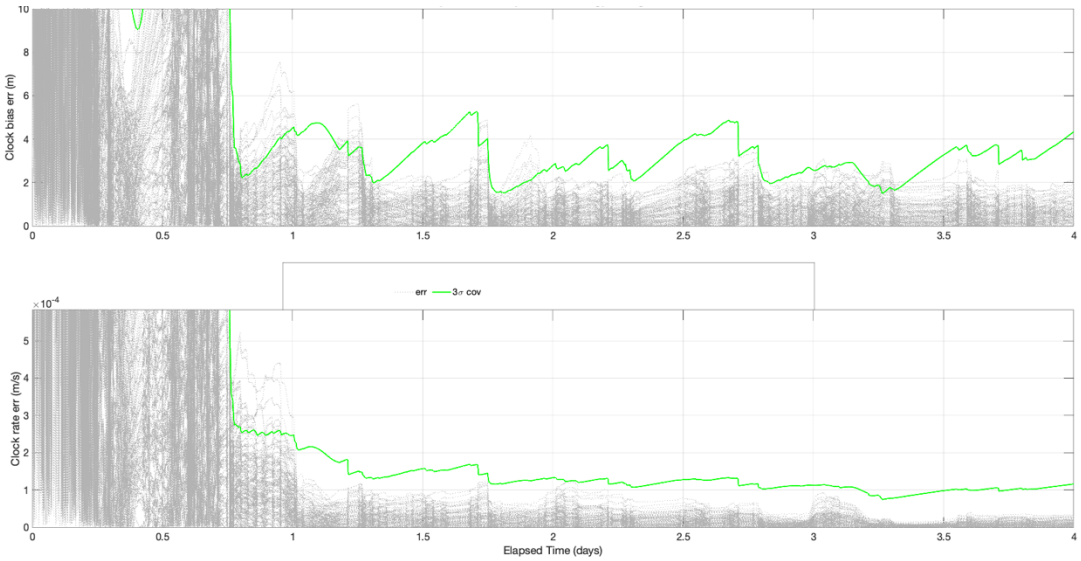


Figure 5: MC clock bias (top) and clock rate (bottom) errors for LNN: RAFS clock, GPS, OpNav CF, and GN measurements



While *Figures 4* and *5* show performance for one clock and measurement set scenario for LNN OD, *Figures 6* and *7* show the maximum and mean state and clock errors, respectively, for the different scenarios of LNN self-OD analyzed. For each label on the x axis, the top row shows the measurements used with CF as shorthand for OpNav center-finding, the middle row shows the on-board clock used, and the bottom row shows "Outage" if a 4-hour GPS outage near Perilune was included. The y-axis is on a log scale. All errors are taken over the last orbit after the filter has converged fully. The max errors are chosen to show the possible extent of the 3-σ errors, though it is not exactly equivalent due to the limited number of MC runs. Additionally, the mean of the RMS position and velocity errors over the last orbit are provided to show typical errors for each case. The MC scenario portrayed in *Figures 4* and *5* is labeled “GPS, CF, GN, RAFS”. All cases shown in *Figures 6* and *7* are sorted by the mean errors.

Figure 6: Relay self-OD position and velocity errors across varied clock and measurement sets

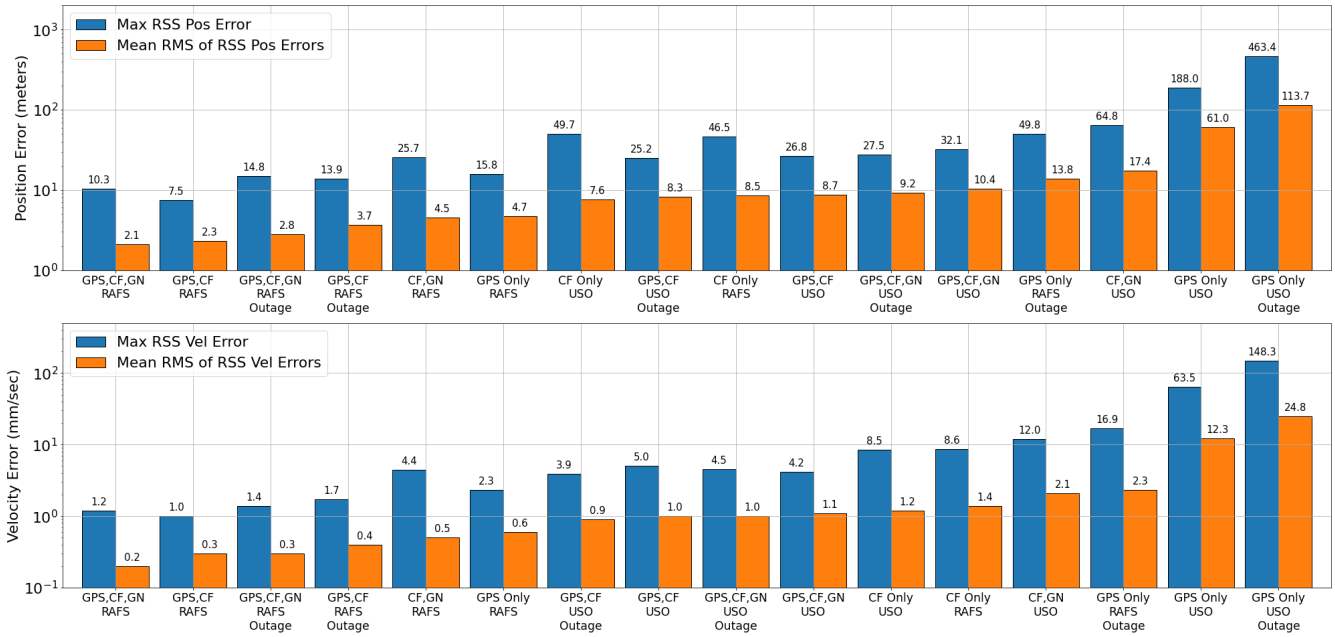
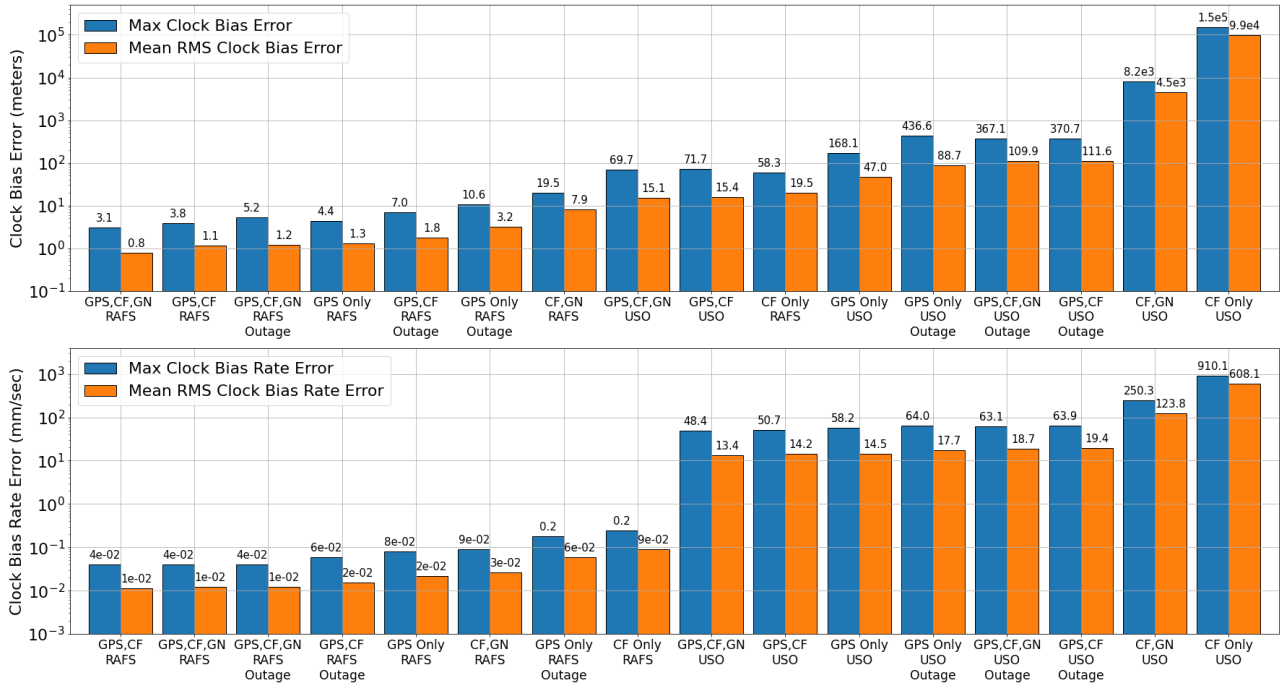


Figure 7: Relay self-OD clock bias and clock bias rate errors across varied clock and measurement sets



LANDER DESCENT OD

Along with MC simulations for the LNN relay self-OD, a variety cases were run for a lander descent to the Lunar surface using 100 MC iterations for each. These simulations have several goals.

1. Assess lander performance using LNN reference signal PR and Doppler measurements and impact of LNN onboard clock on results.
2. Compare and fuse LNN reference signal measurements with other observables for the lander like TRN and GN.

Table 9 shows the inputs for the baseline LNN cases, LNNA and LNNB. Both cases use OpNav CF, GPS and GN measurements in the self-OD**,** but LNNA uses the more accurate RAFS clock while LNNB uses a USO.

Table 9: Relay self-OD cases used for lander descent

Relay Self-OD Case	Clock	GPS Outages	Observables
LNNA	RAFS	None	OpNav CF, GPS, GN
LNNB	USO	None	OpNav CF, GPS, GN

Table 10 shows the MC parameters varied for each lander descent run. The errors were sampled following a Gaussian distribution. The lander onboard filter is assumed to be initialized with a converged solution taken from the NRHO when the lander begins its descent. The initial state and clock errors used for this analysis are based on NRHO OD performance at Apolune from several GGMS runs using a RAFS with GN and line of sight LNN reference signal PR and Doppler measurements. The NRHO navigation analysis is not included in this paper. The parameters estimated for the lander descent MC analysis include the initial state, GN PR biases, LNN reference signal PR biases, clock bias, clock rate, and clock acceleration.

Table 10: Parameters varied each descent MC run

Parameter	Error Applied (1-σ)
Initial Position	100 m
Initial Velocity	1 $\frac{\text{mm}}{\text{s}}$
Initial Clock Bias	10 m
Initial Clock Bias Rate	1e-10 $\frac{\text{m}}{\text{s}}$
Initial Clock Bias Acceleration	1e-15 $\frac{\text{m}}{\text{s}^2}$
Spacecraft Mass	0.96 kg
Spacecraft Area	1 m^2
Spacecraft Cr	0.1
GN PR Bias (per-pass)	15 m

Different metrics are used to assess the lander performance at various points of the descent. These include the state errors at one hour post LOI, the state errors five minutes before touchdown, and the percentage of cases where touchdown is known within a radius of 50 and 100 meters of the targeted landing site. The state estimate one hour after LOI informs the maneuver for descent to the 15x15 km orbit, and the state errors five minutes before touchdown inform the series of maneuvers for landing. An example descent MC error plot is shown in *Figure 8* along with labels for LOI, LOI plus one hour, and touchdown. The MC error plot shows relatively tightly grouped position and velocity errors, no large outliers, and rough adherence to the filter 3-σ error bounds shown in green, though the filter covariance may be a bit too large for most of the simulation. Due to the large number of maneuvers in the descent trajectory, the filter needed to be tuned conservatively using larger process noise and filter measurement multipliers to prevent divergent cases. *Figures 9, 10* and *11* show the results of the descent MC simulations. Several parameters were varied for each of the 11 MC cases which are shown as labels on the x-axis. These parameters include the measurement observables utilized in the top row and the relay self-OD case used (either LNNA or LNNB) on the bottom row of the labels.

Figure 8: MC RSS Position and velocity errors for lander using Xlink, GN and TRN with LNNA

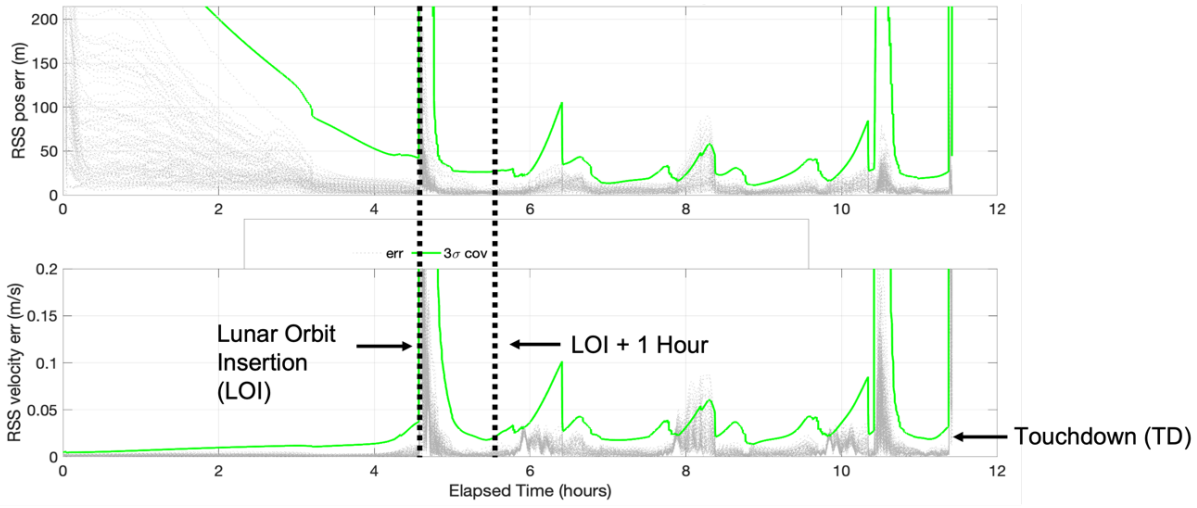


Figure 9: Lander descent MC results one hour post LOI

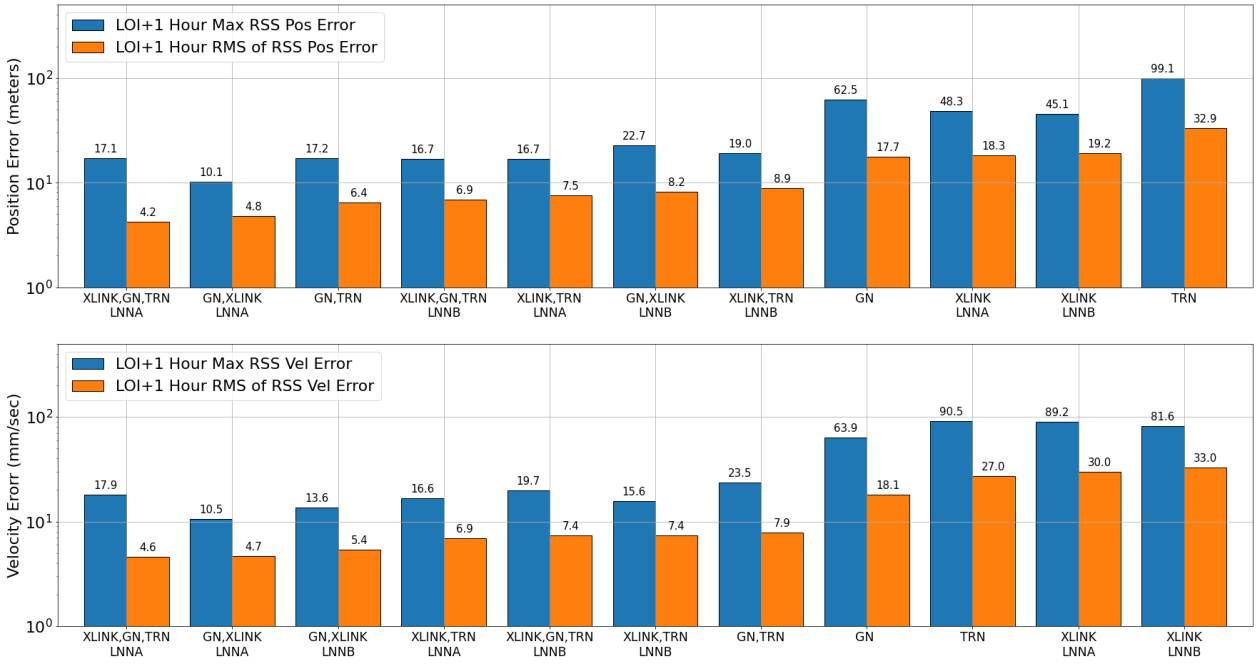


Figure 10: Lander descent MC results five minutes before touchdown

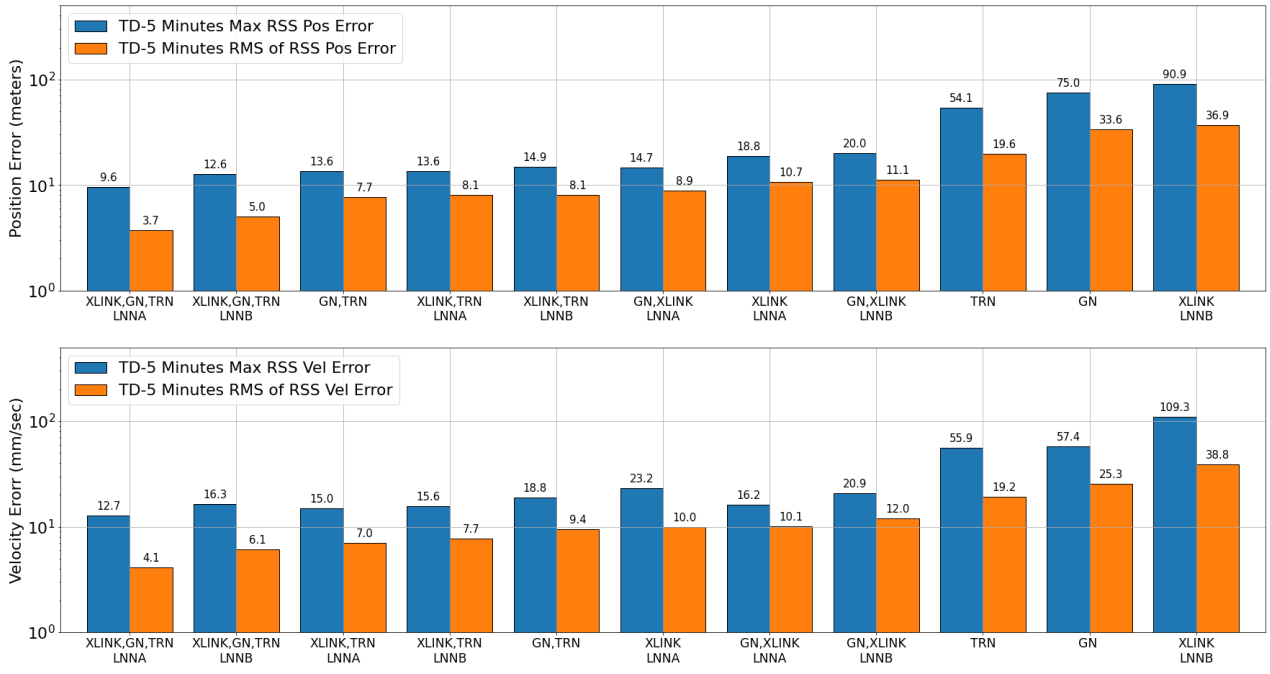
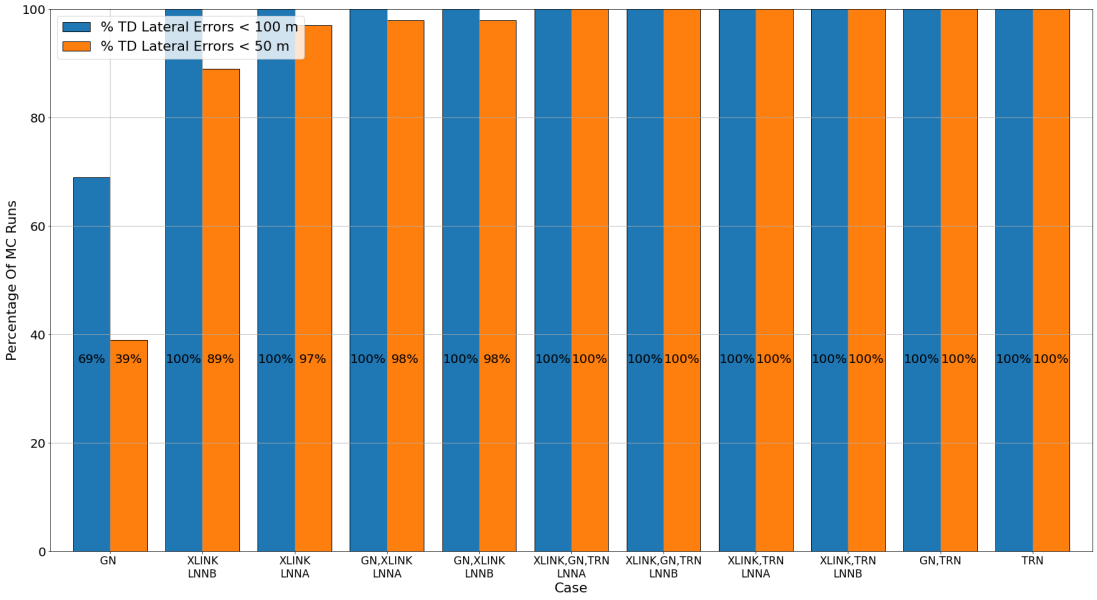


Figure 11: Lander descent MC results at touchdown



DISCUSSION

The LNN relay self-OD MC results show a strong dependence on the on-board clock. For the GPS-only cases the maximum position error increases from 15.8 meters using a RAFS to 188.0 meters using a USO. Much of that error for the USO comes from the clock bias estimate, with a maximum error of 168.1 meters. This difference in performance between the RAFS and USO is even more apparent when GPS outages are included in the GPS-only cases. Both the RAFS and USO GPS-only cases show about three times higher errors when GPS outages are included versus constant GPS coverage, up to 49.8 meters and 463.4 meters, respectively. LNN ephemeris errors at the 500-meter level could quickly add large error signatures to the PR and Doppler measurements on the reference signal broadcast to users, though the impact of the LNN ephemeris errors alone on the provided PR and Doppler measurements requires further analysis. OpNav CF measurements seem to work well by themselves in obtaining an accurate relay position estimate regardless of clock, at 46.5 meters and 49.7 meters respectively for the RAFS and USO cases. However, OpNav CF does not inform clock bias or rate estimates, so the clock errors can quickly grow quite large, especially for the USO which reaches a maximum clock bias error of 150 km or 0.5 milliseconds after four days. OpNav CF and GPS measurements seem to synergize well, with OpNav CF being especially helpful during GPS outages. Using GPS with outages plus OpNav CF observables, the RAFS and USO cases have maximum position errors of 13.9 meters and 25.2 meters, respectively. Still, the clock bias errors grow quite large, to around 370 meters or about 1 microsecond for the USO case. Even with the addition of ground station measurements, the maximum clock bias errors only reduce to 367.1 meters for the USO. These results suggests that to avoid large LNN ephemeris and clock errors that could bias or degrade the PR and Doppler measurements provided by the LNN reference signal, a RAFS type clock is necessary. Additionally, adding OpNav CF measurements adds resilience in estimating the LNN state during GPS outages. When GPS measurements are available along with OpNav CF measurements, GN measurements do not appear very helpful in determining the state and clock errors, though this analysis only used four hours of GN tracking time per day. GN could be more helpful, especially in determining the clock errors, given more tracking time. Future analysis will analyze including GPS Doppler and TRN observables to improve performance.

The descent MC results show the effects of various combinations of LNN reference signal PR and Doppler, TRN and GN measurements on navigation performance. The descent case using only TRN measurements shows very good landing accuracy given ideal illumination conditions, with 100% of the MC cases falling within 50 meters of the landing site but results in a maximum position error of 99.1 meters one hour after LOI where the OpNav measurements transition from CF to TRN, and 54.1 meters five minutes before the series of terminal descent maneuvers. Given the 60-second cadence of the OpNav update, if several images are not able to be processed successfully, the state errors five minutes before touchdown could propagate and introduce large landing errors. While the descent case using only GN observables shows similar state errors at LOI and five

minutes before touchdown compared to the LNNA-only and TRN-only cases respectively, only 39% of MC runs fall within 50 meters of the landing site at touchdown. Using measurements from the LNNA reference signal, the maximum position errors at one hour past LOI and five minutes before touchdown are 48.3 meters and 18.8 meters, respectively, much better than the TRN only case, while showing slightly worse landing performance than the TRN only case with 97% of cases falling within 50 meters of the landing site. Descent using only observables from LNNB shows similar errors to the LNNA case at one hour past LOI, but much larger errors at five minutes before touchdown with a maximum position error of 90.9 meters. Additionally, only 89% of cases fall within 50 meters of the landing site versus 97% when using measurements from LNNA. When combined with other measurement types, the LNN reference signal measurements greatly increase navigation performance when using LNNA or LNNB. Compared to the TRN only case, adding LNN reference signal measurements to the TRN observables results in much lower state errors at one hour past LOI and five minutes before touchdown for both the LNNA and LNNB cases. When GN, TRN and LNN reference signal measurements using LNNA are combined, performance is quite good with max RSS position errors at one hour past LOI and five minutes before touchdown of 17.1 and 9.6 meters respectively with 100% of cases landing within 50 meters of the landing site. The same combination of observables using LNNB shows similar performance with maximum position errors of 16.7 meters and 12.6 meters at one hour past LOI and five minutes before touchdown respectively and 100% of cases landing within 50 meters of the landing site. While the LNN relay could provide useful measurements using an onboard RAFS or USO, especially when those measurements are used alongside other measurement types, the usefulness as the sole measurement observable is highly dependent on the onboard clock. This seems to be mainly the results of clock bias errors adding large biases to the provided PR measurements, though further analysis is needed to study the effects of the LNN clock bias or LNN ephemeris errors alone on the provided measurements. When other concurrent observables like TRN are incorporated, these biases can be estimated effectively which reduces the effect of the large PR biases. The complementary nature of the multiple measurements enables a robust and resilient solution.

CONCLUSION

This study found that the choice of onboard clock and measurement observables used on a potential Lunar relay has a large impact on the spacecraft state and clock errors and the accuracy of measurements provided to users. While the spacecraft state errors are only 2-3 times larger using an onboard USO instead of RAFS, the USO clock errors can grow much larger, especially during GN and GPS measurements outages. Including OpNav CF measurements during GPS outages was shown to be sufficient to maintain the spacecraft state knowledge using both the RAFS and USO clocks but does not help with the clock error estimation. A combination of GPS and OpNav CF observables with a RAFS clock was shown to provide precision navigation performance, even throughout measurement outages. It was also shown that the relay state and clock errors have a direct effect on the navigation for a Lunar lander using LNN reference signal PR and Doppler measurements, as expected. When combined with TRN and GN measurements, the LNN reference signal measurements greatly improve descent performance regardless of the relay onboard clock, but when used as the sole measurement observable, the choice of relay onboard clock was shown to have a large degrading effect. To maximize the potential for a Lunar relay as a compliment and alternative to TRN measurements, a RAFS type clock is suggested onboard the relay, though a relay with a USO clock could still provide useful measurements. Future work needs to be done to study other relay user cases, and to assess the impact and sensitivity of user performance to relay ephemeris and clock errors.

REFERENCES

1. Israel, D. J., "Draft LunaNet Interoperability Specification", https://esc.gsfc.nasa.gov/projects/TEMPO?tab=lunanet, 2021.
2. Israel, D. J., Mauldin, K. D., Roberts, C. J., Mitchell, J. W., Pulkkinen, A. A., La Vida, D. C., Johnson, M. A., Christe, S. D., and Gramling, C. J., "LunaNet: a flexible and extensible lunar exploration communications and navigation infrastructure", *IEEE Aerospace Conference*, 2020, pp. 1-14.
3. Long, A.*, Goddard Enhanced Onboard Navigation System (GEONS) Mathematical Specifications,* Release 3.0, January 2019.
4. Winternitz, L. B., Bamford, W. A., Price, S. R., Carpenter, J. R., Long A. C., and Farahmand M., "Global positioning system navigation above 76,000 km for NASA's magnetospheric multiscale mission", *Journal of the Institute of Navigation*, July 2017, vol. 64, pp. 289-300.
5. Miller, J. J. and Parker, J. K., "NASA Update to WG-B: MMS GPS Performance at 29.34 Re (50% of Way to the Moon)", 2019, https://ntrs.nasa.gov/citations/20190027307, Accessed: 2021-12-16.

6. Schlenker, L. G., Parker, J. K., Bauer, F. H., Winternitz, L. B., Long A. C., Craft K. J., and Hassouneh M. A., "Applications and Benefits of GNSS for Lunar Exploration", 2021, https://ntrs.nasa.gov/citations/20210014051, Accessed: 2021-12-23.
7. Donaldson, J. E., Parker, J. K., Moreau, M. C., Highsmith, D. E., and Martzen, P. D., "Characterization of on-orbit GPS transmit antenna patterns for space users", *Journal of the Institute of Navigation,* 2018, vol. 67*,* pp. 411-438.
8. Teunissen, P. J., Montenbruck, O., *Springer handbook of global navigation satellite systems,* 2017, vol. 1, New York, NY, USA: Springer International Publishing.
9. Rizk, B., d'Aubigny, C. D., Golish, D., Fellows, C., Merrill, C., Smith, P., Walker, M. S., Hendershot, J. E., Hancock, J., Bailey, S. H., and DellaGiustina D. N., "OCAMS: the OSIRIS-REx camera suite", *Space Science Reviews*, 2018, vol.214, pp.1-55.
10. Hutsell, S. T., W. Reid, G., Crum, L. J. D., Mobbs, L. H. S., and Buisson, J. A., "Operational use of the Hadamard variance in GPS", *Proceedings of the 28th Annual Precise Time and Time Interval Systems and Applications Meeting*, 1996, pp. 201-214.
11. Lemoine, F. G., Goossens, S., Sabaka, T. J, Nicholas, J. B., Mazarico, E., Rowlands, D. D., ... and Zuber, M. T., "GRGM900C: A degree 900 lunar gravity model from GRAIL primary and extended mission data", *Geophysical research letters*, 2014, vol. *41*, pp. 3382-3389.
12. Folkner, W. M, Williams, J. G., & Boggs, D. H., "The planetary and lunar ephemeris DE 421", *IPN progress report*, 2009, vol. 42, pp. 1-34.